Inorganic−Organic Hybrid Vesicles with Counterion- and pH-Controlled Fluorescent Properties

Dong Li,[†,§] Jie Song,[‡,§] Panchao Yin,[†] Silas Simotwo,[†] Andrew J. Bassler,[†] YuYu Aung,[†] James E. Roberts,[†] Kenneth I. Hardcastle,[‡] Craig L. Hill,*[,‡] and Tianbo Liu*[,†]

[†]Department of Chemistry, Lehigh University, Bethlehem, Pennsylvania 18015, United States
[‡]Department of Chemistry, Emory University, Atlanta, Georgia 30322, United States

S *Supporting Information*

ABSTRACT: Two inorganic−organic hybrid clusters with one or two covalently linked pyrene fluorescent probes, $[(n\text{-}C_4H_9)_4N]_2$-$[V_6O_{13}\{(OCH_2)_3C(NH(CO)CH_2CH_2CH_2C_{16}H_9)\}\{(OCH_2)_3$-$C-(NH_2)\}]$ $((TBA^+)_2\mathbf{1})$ and $[(n\text{-}C_4H_9)_4N]_2[V_6O_{13}\{(OCH_2)_3$-$C(NH(CO)CH_2CH_2CH_2C_{16}H_9)\}_2]$ $((TBA^+)_2\mathbf{2})$, respectively, are synthesized from Lindqvist type polyoxometalates (POMs). The incorporation of pyrene into POMs results in amphiphilic

hybrid molecules and simultaneously offers a great opportunity to study the interaction between hybrid clusters and their counterions. 2D-NOESY NMR and fluorescence techniques have been used to study the role of counterions such as tetrabutyl ammonium (TBA) in the vesicle formation of the hybrid clusters. The TBA^+ ions not only screen the electrostatic repulsions between the POM head groups but also are involved in the hydrophobic region of the vesicular structure where they interrupt the formation of pyrene excimers that greatly perturbs the luminescence signal from the vesicle solution. By replacing the TBA^+ counterions with protons, the new vesicles demonstrate interesting pH-dependent fluorescence properties.
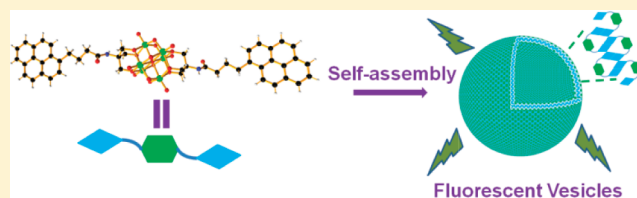
INTRODUCTION

Smart supramolecular assemblies that respond to single or multiple external stimuli, such as temperature,[1] ionic strength,[2] pH,[3] redox,[4] light,[5] ultrasound,[6] and magnetic field,[7] are of great interest for their potential applications in drug delivery, oil recovery, and design of new sensors and catalysts.[8−13] While most smart supramolecular assemblies are constructed from organic molecules or block copolymers, incorporating functional inorganic components (such as quantum dots, silica, transition metal ions, etc.) into organic building blocks to make functional hybrid assemblies represents an interesting new direction.[5,6,14] Polyoxometalates (POMs), a large group of early transition metal oxide clusters, represents structurally well-defined inorganic molecules with diversified structures and properties.[15−17] The synergistic combination of POMs and organic components gives these hybrids noteworthy properties of potential utility.[18,19] For instance, polymers with grafted POMs can be used in photovoltaic cells or in trapping magnetic nanoparticles,[20,21] and surfaces that are covered with hybrid POMs (SAM−POM−pyrene) show specific cell adhesion ability.[22] Organo-POM hybrids[23−27] have been shown to exhibit unusual spectroscopic properties[28] or catalyze oxidation reactions,[29−31] organometallic POM clusters have been tested for norbornene and cyclohexene oxygenation as precatalysts,[32] and a recent study on a photoresponsive surfactant-encapsulated POM complex has shown an interesting dynamic structure transition in solution.[33] The new hybrids with surfactant-like amphiphilic solution properties are particularly interesting because they can be compatible with both hydrophilic and hydrophobic

environments and therefore can enhance the applications of the functional clusters. Interesting supramolecular structures such as micelles, vesicles, liquid crystals, and 2D-films have been reported in various amphiphilic hybrid solutions.[34−36] The self-assembly is dependent upon solvent polarity,[37] the hydrocarbon chain length,[38] the type and length of organic linkers,[39] and the architecture of the hybrids, as well as temperature.

Meanwhile, the development of fluorescent tags or probes opens new opportunities for smart molecules. Applying fluorescent probes to investigate biochemical microenvironments is a powerful technique that can often provide unique and critical information. Pyrene, a highly symmetrical polyaromatic hydrocarbon fluorophore possessing restricted modes of motion, can exhibit fine structure in its absorbance and fluorescence spectra at room temperature.[40] One important application of the pyrene fluorescence stems from its ability to probe the polarity of the local microenvironment, either in a hydrophobic or hydrophilic media, from the change of specific emission peaks in the spectrum.[41,42] Therefore, amphiphilic hybrid POM clusters with pendent pyrene fluorescent probes are of potential interest for the construction of smart supramolecular assemblies via macro-ion-counterion interaction.

It is an interesting question how the hybrid surfactants arrange themselves to form closely packed regions in the supramolecular structures. These hybrids differ from conventional surfactants in

that they have large polar head groups making close packing of hydrophobic domains very difficult due to the spatial obstruction. We proposed, but without solid evidence, that the counterions might be important by perturbing the solvophobic layer formation.[39] The newly synthesized hybrid clusters with pyrene as fluorescent probes offer a unique opportunity to study this phenomenon.

■ EXPERIMENTAL SECTION

X-ray Crystallography. X-ray quality crystals of $[V_6O_{13}\{(OCH_2)CNH_3\}]$·2.4DMSO (NH_3V_6), $[(n-C_4H_9)_4N]_2[V_6O_{13}\{(OCH_2)_3CNH_2\}_2]$ $(TBA-NH_2V_6)$, and $(TBA^+)_2$**2** were coated with Paratone N oil and mounted on a small fiber loop for index and intensity data collection. The X-ray diffraction data were collected under a nitrogen stream at 173 K on a Bruker D8 SMART APEX CCD single-crystal diffractometer with graphite monochromated Mo Kα (λ = 0.71073 Å) radiation. Data collection, indexing, and initial cell refinements were processed using the SMART[43] software while frame integration and final cell refinements were carried out using the SAINT[44] software. The final cell parameters were determined from the least-squares refinement of total reflections. The structures were determined through direct methods (SHELXS97) and difference Fourier maps (SHELXL97). The final results of crystal data and structure refinement are summarized in Table S1 of the Supporting Information. The Cambridge Crystallographic Data Centre deposition number for NH_3V_6, $TBA-NH_2V_6$, and $(TBA^+)_2$**2** are CCDC 821763, 821764, and 821765, respectively.

Cation Exchange. Counterion replacement of TBA^+ with H^+ was achieved by using a cation-exchange resin column. For a typical experiment, 5 mg of hybrid cluster **1** or **2** was dissolved in 2 mL of acetonitrile. This solution was then applied to a prepacked, cation-exchange resin column (Amberjet 1200 hydrogen form purchased from Sigma-Aldrich) rinsed with D.I. water and acetonitrile. An additional 20−50 mL of acetonitrile was used to elute the column, and the yellow fraction was collected. The post elution was further washed with 5 mL of diethyl ether to remove organic impurities. The final solution was transferred into a glass culture plate and kept in the dark for several days to fully evaporate the solvent. Yellow colored fine powders were collected and could be easily dissolved in water or DMSO for further study.

Laser Light Scattering. Both dynamic light scattering (DLS) and static light scatting (SLS) techniques were used to characterize the self-assembly of hybrids in solution. A Brookhaven Instruments Inc. light scattering spectrometer, equipped with a diode-pumped solid-state (DPSS) laser operating at 532 nm and a BI-9000AT multichannel digital correlator was used for all experiments. The SLS was performed over a broad range of scattering angles from 30° to 130°, with a 2° interval. The radius of gyration (R_g) and the weight-average molecular mass (M_w) of the large assemblies were calculated using the Rayleigh−Gans−Debye equation:[45]

$$Hc/R_{90} = 1/M_w + 2A_2*c \qquad (1)$$

where H is an optical parameter, M_w is the weight-average molecular mass of the solutes, A_2 is the second virial coefficient, and c is the solute concentration. The $2A_2c$ term is neglected during calculations because the sample solutions examined in this study have very low concentrations.

For DLS measurements, the intensity−intensity time correlation functions were analyzed by the constrained regularized (CONTIN) method in order to ascertain the average hydrodynamic radius (R_h) of the large assemblies. The average apparent translational diffusion coefficient, D_{app}, was determined from the normalized distribution function of the characteristic line width, $\Gamma(G)$. The hydrodynamic radius R_h is converted from D through the Stokes−Einstein equation:

$$R = k_B T/6\pi\eta D \qquad (2)$$

where k_B is the Boltzmann constant and η is the viscosity of the solvent at temperature T. The particle size distribution in solution can be obtained

by plotting $\Gamma G(\Gamma)$ versus R_h, with $\Gamma_i G^i(\Gamma^i)$ being proportional to the angular-dependent scattered intensity of particle i having an apparent hydrodynamic radius $R_{h,i}$. The temperature in the sample chamber was controlled to within ±0.1 °C. More details about SLS and DLS can be found in our previous publications.[46]

Transmission Electron Microscopy (TEM). Samples for electron microscopy characterization were prepared by pipeting 5 μL of diluted solution onto a carbon-coated TEM grid. The TEM samples were left under ambient conditions for several hours until the solvent completely evaporated. Bright-field (BF) TEM imaging was performed on a JEOL 2000FX transmission electron microscope having an accelerating voltage of 200 kV.

Zeta (ζ) Potential Analysis. All the ζ potential analysis measurements were performed on a Brookhaven Instrument Inc. Zeta PALS Analyzer. The instrument is equipped with a red laser operating at 660 nm wavelength and has an accuracy of ±2% for filtrated samples. The sample chamber was kept at 25 ± 0.1 °C, and all sample solutions were loaded 30 min prior to measurements in order to achieve thermal equilibrium with the chamber.

Nuclear Magnetic Resonance Spectroscopy (NMR). All 1D and 2D ^1H NMR measurements in the liquid state were performed on a Bruker Avance 500 spectrometer equipped with a 5 mm triple-axis gradient (TXI) probe. 2D nuclear Overhauser enhancement spectroscopy (2D NOESY) spectra were recorded with 256 t_1 increments and 64 scans under the pulse program of noesygpph19 provided with Topspin 1.3. The relaxation delay D1 varied from 1 to 2 s, and the mixing time D8 changed from 0.1 to 0.5 s. Baseline correction and noise reduction were performed when appropriate. All spectra were taken at room temperature, and FIDs were processed and analyzed with the NMR software provided by Bruker.

Fluorescence Measurements. Fluorescence spectra were recorded at room temperature on a Cary Eclipse fluorescence spectrophotometer. The excitation wavelength, λ_{exc}, used was 335 nm, and the spectrum width was from 350 to 700 nm. An emission filter of 360−1100 nm was used. Each spectrum was obtained by averaging three scans and corrected for scatter of the equivalent blank sample. In calculations of the excimer-to-monomer intensity ratio, the monomer (I_M) and the excimer (I_E) were determined by taking the integrals under the fluorescence peaks from 350 to 430 nm for the pyrene monomer and from 430 to 700 nm for the pyrene excimer.[40]

■ RESULTS AND DISCUSSION

Synthesis and Characterization of Hybrid $(TBA^+)_2$1 and $(TBA^+)_2$2. The detailed synthesis and purification procedure for precursors and hybrid clusters can be found in the Supporting Information. The synthetic protocol was developed here to efficiently construct a new type of POM-based inorganic−organic hybrid. Based on the idea that succinate (NHS) esters show high reaction selectivity to N-termini in negatively charged protein modification, the primary amine groups symmetrically attached on the two opposite faces of a negatively charged hexavanadate were further functionalized by reacting with a pyrene-containing succinate ester (PASE) at room temperature, to give the desired hybrids via efficient amide bond formation. By tuning the PASE/TBA−NH_2V_6 molar ratio in the reaction, asymmetric hybrid compounds, **1** (only one amine group reacted), and symmetric hybrid compounds, **2** (both of two amine groups reacted), were obtained, respectively, in high yield and selectivity.

Their molecular structures were determined from single crystal X-ray diffraction, ^1H, ^{13}C NMR, IR, and elemental analysis (see Scheme S1 and Part 1 in the Supporting Information). Analysis of the packing in the unit cells of $(TBA^+)_2$**2** shows several
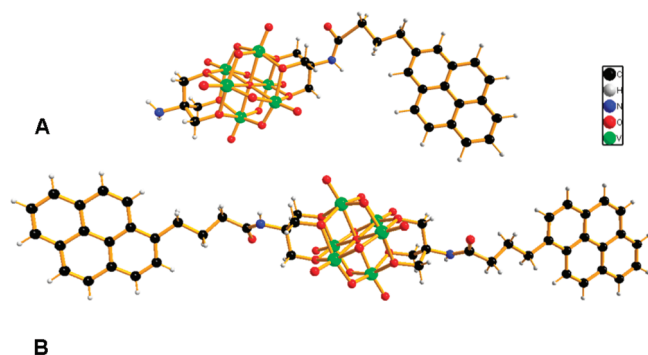
[a] Atoms are represented as follows: V (green), N (blue), O (red), C (black), H (white).

supramolecular interactions between the polyanions in solid state, which include limited pyrene—pyrene π stacking (the closest distance between two adjacent carbons on two pyrene rings is ca. 0.335 nm) and H bonding between the amide —NH— and a terminal POM oxygen (the N...O distance is ca. 0.286 nm) (Figure S2 of the Supporting Information). Such interactions could well be operable in the vesicles and are expected to play a role in solution aggregation. The length of the hydrophobic region is critical to the overall amphiphilic property of the hybrid cluster as well as the self-assembled supramolecular structures.[38,47−49] At the same time, POMs are well-known electron acceptors so fluorescence quenching by the clusters was a concern at the outset.[50] Therefore, we targeted complexes in which the pyrene fluorophores were separated from the POM head groups by a four-carbon hydrocarbon chain. Later, we determined that this hydrocarbon chain maintains flexibility in the hydrophobic component and also preserves the pyrene fluorescence.

Characterization of the Amphiphilic Properties of Hybrids 1 and 2 in Polar Solvents. As shown in Scheme 1, two novel POM based inorganic—organic hybrids are constructed by incorporating one or two pyrene functional groups onto one Lindqvist-type polyoxovanadate $[V_6O_{13}\{(OCH_2)_3CNH_2\}]^{2-}$. The linkage of flexible, hydrophobic organic tails to the inorganic POM head groups renders these new species amphiphilic. Hybrids $(TBA^+)_2\mathbf{1}$ and $(TBA^+)_2\mathbf{2}$ are insoluble in water but can be readily dissolved in dimethyl sulfoxide (DMSO), dimethyl formamide (DMF), and other polar organic solvents. For 0.1 mg/mL of hybrid $(TBA^+)_2\mathbf{1}$ in DMSO, a very low scattered intensity (∼45 Kcps) was collected from SLS measurements (for comparison, the scattered intensity of pure solvent is ∼40 Kcps), indicating that the hybrid molecules prefer to remain as monomers in solution rather than large assemblies. However, when additional water was introduced to make a solvent containing up to 70 vol% water, the total scattered intensity starts to increase significantly, and supramolecular structures are observed under DLS, as shown in Figure 1. The CONTIN analysis of the DLS measurement on this solution reveals a peak corresponding to assemblies with a very narrow size distribution and an average hydrodynamic radius (R_h) of 50 nm. The R_h value does not show angular dependence that suggests that the supramolecular structures are likely spherical.[45] The radius of gyration (R_g) of the assemblies measured by SLS is 48 nm (see the Supporting Information). The relation of $R_{h,0} \approx R_g$ strongly suggests that

the supramolecular structures have a hollow spherical vesicular structure, which is also clearly confirmed by the TEM studies (Figure 1C). The TEM image shown in Figure 1D reveals several important aspects. First, the different contrast shown inside (lighter color) and around (darker color) the vesicular structures indicate they are hollow, which is quite similar to the vesicles formed by phospholipids.[51] Second, these vesicles collapsed on the carbon film due to the evaporation of internal solvent under high vacuum condition, indicating a soft and flexible nature of the vesicles' membrane. In order to form such vesicular structures in the mixed solvents as shown here, it is reasonable to assume that the hybrids use their polar POM clusters to face the hydrophilic solvent while their organic tails form a hydrophobic domain. The addition of water induces dissociation of the TBA^+ counterions from the POM cluster and increases the overall negative charge on the polar head groups, which in turn changes the amphiphilicity of the hybrid molecules and leads to the vesicle formation. The above discussions focus on one set of condition (0.1 mg/mL hybrid **1** in 80:20 v/v water/DMSO); however, similar vesicular structures are also observed in different solvents, that is, in water/acetonitrile, or in water/methanol.

When the original TBA^+ counterions of **1** are replaced by tetraethylammonium (TEA^+) or tetramethylammonium (TMA^+), similar vesicular structures were observed. However, compared with the case of TBA^+, the total scattered light intensity becomes lower, and more water is needed to trigger the vesicle formation. The R_h of the large vesicular structures also changes from 50 to 30 nm and 23 nm in the same solvent system (80:20 v/v H_2O/DMSO) (Figure 1A and B), respectively. The decrease of the vesicle size should be attributed to the shorter alkyl chains of the counterions, which decreases the size of the hydrophobic domain and consequently increases the curvature of the vesicles. These results indicate that the counterions play an important role in regulating the amphiphilic nature of the hybrid clusters and the electrostatic interactions between them.

Hybrid $(TBA^+)_2\mathbf{2}$ in mixed solvents (H_2O/DMSO, H_2O/acetonitrile, etc.) shows similar self-assembly behavior as hybrid $(TBA^+)_2\mathbf{1}$. However, the vesicular structures formed by hybrid **2** are smaller than those formed by hybrid **1** under the same conditions. This is because an additional bending energy is needed to properly fold the two hydrophobic tails of hybrid **2** into the vesicular structure and therefore leads to a higher curvature or smaller vesicles (see the Supporting Information).[52]

Counterions Affect the Packing of Hybrid Clusters in Vesicles. Fluorescent probes are highly useful in monitoring polarity changes of microenvironments in macromolecules and membranes. The general dependence of probe fluorescence on polarity has been attributed to the dipole—dipole interaction between the singlet excited state of the fluorophores and the solvent molecules. Specifically, the fine structural pattern in the fluorescence of the pyrene monomers is found to be independent of excitation conditions or collisional quenching but highly dependent on solvent polarity.[42] Therefore, any changes in the pyrene fluorescence will reveal interactions between counterions and the hybrid clusters. As shown in Figure 2, when counterions are TBA^+, TEA^+, or TMA^+, the fluorescence intensity primarily comes from the pyrene monomer, and no excimer peak is observed. Under these conditions, vesicular structures have already formed in the solution. Therefore, the fluorescence spectra indicate that the pyrene groups on the vesicle surface are not spatially close enough to form excimers. However, the fluorescence spectra are significantly different when H^+ counterions are present
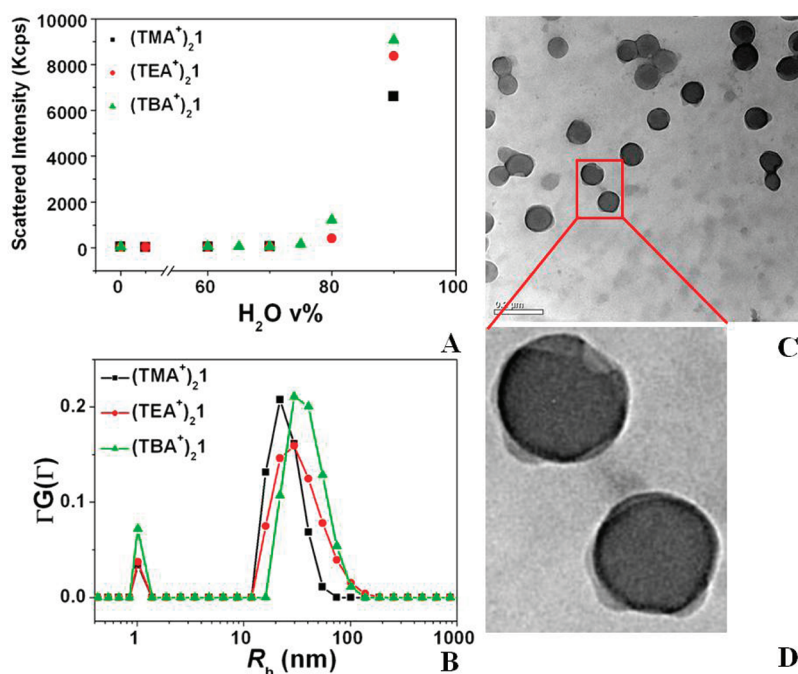
Figure 1. (A) Total scattered intensity recorded by SLS for hybrid cluster **1** with different counterions in H_2O/DMSO mixed solvents. (B) CONTIN plot of the size distribution of vesicular structures formed by hybrid cluster **1** with different counterions in 80:20 v/v H_2O/DMSO mixed solvents. (C) TEM image of the vesicular structure formed in 80:20 v/v H_2O/DMSO mixed solvents (bar = 0.2 μm). (D) Enlarged region of **C** in order to show the structural details of the hollow spherical vesicular structures.

in the solution. The emission peaks of the monomer become less well-defined, and the peak of the excimer centered at 480 nm becomes the dominant one for both $H_2\mathbf{1}$ and $H_2\mathbf{2}$. Second, it has been shown in the literature that the polarity of the microenvironment around the pyrene group is reflected by the ratio of the emission peak at 375 nm to the peak at 395 nm: the lower the ratio, the less polar the pyrene environment.[40,41] Figure 2B clearly shows that the pyrene groups are more solvated when large counterions (for example TBA^+) are present in the assemblies. In contrast, when H^+ ions are the counterions, the pyrene groups stay closer to each other. This data confirms that counterions with long alkyl chains can prevent the close packing of the hybrid clusters in the vesicular structures.

More direct evidence comes from the 2D NOESY NMR measurements. In general, when a saturated or inverted proton undergoes dipolar cross-relaxation, another spatially close proton may experience an intensity enhancement, a common phenomenon termed the nuclear Overhauser effect (NOE).[53] The NOE is unique among the NMR phenomena because it does not rely on through-bond J couplings but depends only on the spatial proximity between protons.[54,55] In other words, the strength of the NOE can be used to estimate how close two protons are.[56,57] In the current system, there are two possible scenarios for TBA interaction with the vesicular structure, either strongly bound to the vesicles or as free counterions in solution. Since no covalent chemical bonds are present between TBA cations and the hybrid cluster, it is quite possible that a dynamic exchange and equilibrium exists between bound and free cations. Free TBA cations show very weak to no NOE, while the bound TBAs are explicitly revealed through strong, negative NOE cross peaks. Moreover, the strong, negative NOE from bound TBA cations will outweigh that from free cations and dominate the NOESY spectrum, even when the free TBAs are in considerable excess.[54] Figure 3 shows

that in a 0.25 mg/mL $(TBA)_2\mathbf{1}$ solution in pure DMSO-d_6, the TBA protons exhibit positive NOE cross peaks between adjacent protons indicating that the TBA counterions exist as free ions. The NOE cross peak pattern is identical to that of the control compound TBAI (tetrabutylammonium iodide). This is because there is no vesicle formation in solution. The TBA counterions interact with the $\{V_6O_{19}\}^{2-}$ POM portion through electrostatic interactions. However, when vesicular structures form in 90:10 v/v D_2O/DMSO-d_6 solution, the NOE spectra for $(TBA^+)_2\mathbf{1}$ dramatically changes. First, the previously positive NOE cross peaks become negative, indicating strong binding between the TBA cations and the vesicles. More interestingly, a set of new negative NOE cross peaks appears between cations and the fluorescent pyrene groups on **1** (Figure 3D), which do not appear in Figure 3B. This clearly indicates that the amphiphilic TBA cations interact with the hydrophobic domains in the vesicles. It is almost certain that this interaction interrupts the formation of pyrene excimers that in turn greatly affects the fluorescence pattern of the pyrene (Scheme 2). Previously, we noticed that the dumbbell shaped POM hybrids could form vesicles in water/acetone mixed solvents.[39] The interesting question is how these hybrids could form closely packed hydrophobic layers in their vesicles. The giant POM head groups make the close packing of the alkyl chains very difficult due to spatial hindrance. We speculate that the alkyl chains of the TBA cations interact with the hydrophobic domains, but there is no direct evidence for this. From the 2D NOESY NMR study, we can confirm that the amphiphilic TBA cations are distributed partly into the hydrophobic regions of the vesicular structures.

pH Sensitive Vesicles. When two pyrene groups are spatially close to each other (less than 0.5 nm) without any interruption, an excimer peak appears.[40] We have shown earlier in the paper that replacement of the original TBA counterions by H^+ through
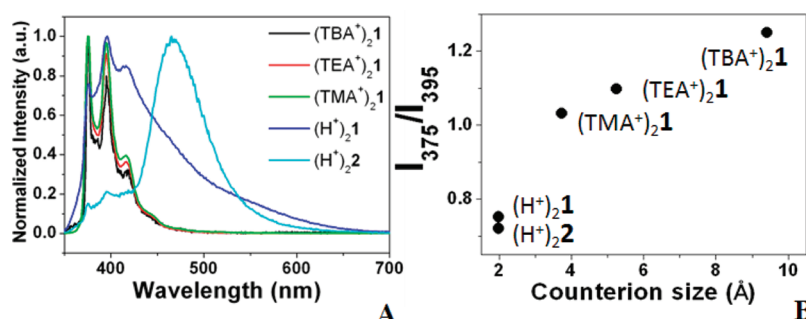
Figure 2. (**A**) Fluorescence spectra of hybrid clusters **1** and **2** with different counterions. (For the TBA, TEA, and TMA salts, the sample concentrations are all at 0.1 mg/mL, and the solvent is 80:20 v/v H_2O/DMSO; for the H salt, the sample concentrations are at ∼0.4 mg/mL, and the solvent is H_2O.). (**B**) Plot of the pyrene monomer fluorescence peak I(375 nm)/I(395 nm) versus the counterion size for hybrid clusters **1** and **2** with different counterions.

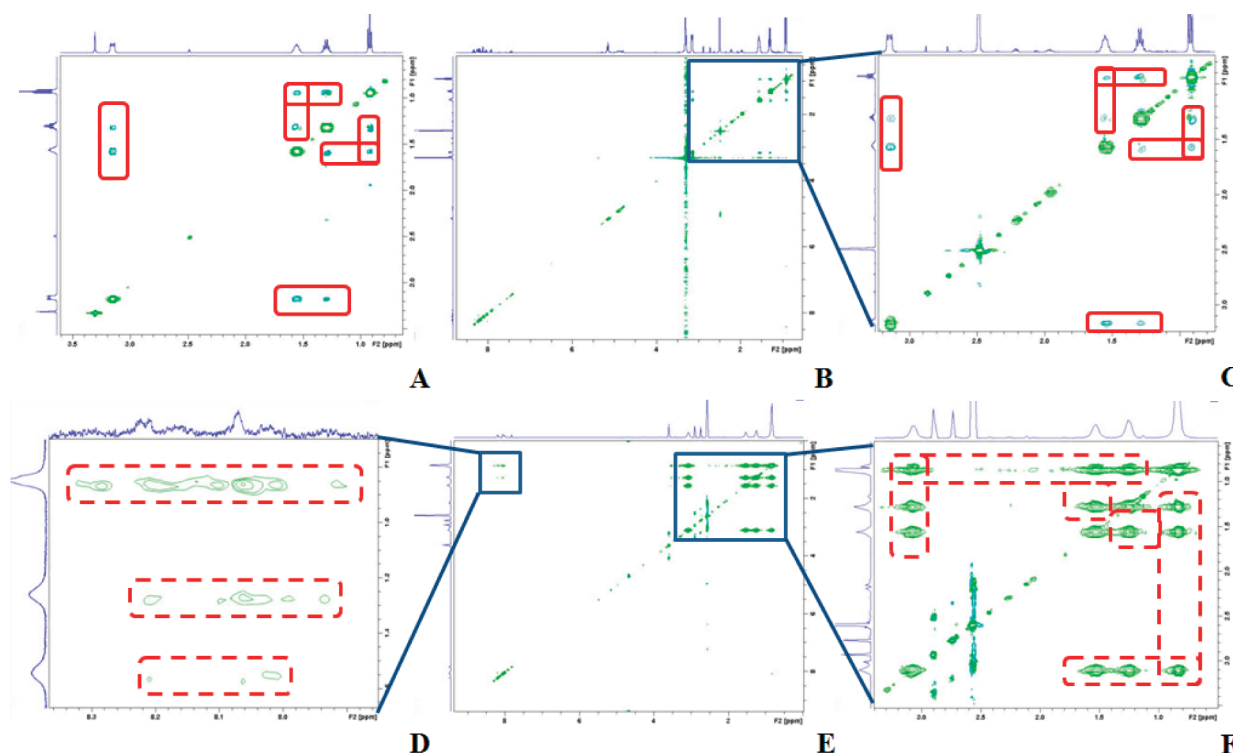**Figure 3.** (**A**) 2D NOESY spectrum of TBAI in DMSO-d_6. (**B**) 2D NOESY spectrum of 0.25 mg/mL (TBA$^+$)$_2$**1** in DMSO-d_6. (**C**) Enlarged region of **B** showing the TBA cross peaks. (**D**) Enlarged region of **E** showing the TBA−pyrene cross peaks. (**E**) 2D NOESY spectrum of 0.2 mg/mL (TBA$^+$)$_2$**1** in 90:10 v/v D_2O/DMSO-d_6 mixed solvent. (**F**) Enlarged region of **E** show the TBA cross peaks. (Important positive NOE peaks with dark green color are highlighted in solid red rectangular while important negative NOE peaks with light green color are highlighted in dashed red rectangular.).

cation exchange changes the fluorescence spectra of the appended pyrene: the peaks due to pyrene excimers become dominant relative to those from pyrene monomers, indicating a much closer packing of the hybrid clusters in the vesicular structure. This unique property gives us a great opportunity to construct a smart, pH sensitive vesicular structure and to study the effect of pH on the assembly and disassembly of vesicular structures. Figure 4 shows that the initial pH for an aqueous solution of hybrid cluster **2** (ca. 0.44 mg/mL based on UV absorption calibration) after counterion exchange is 3.41 and the dominant fluorescence comes from the pyrene excimers. The molar ratio of hybrid **2** divided by free H$^+$ in solution is 0.87 based on solution pH, which indicates only a portion of the H$^+$

ions are released into solution and contribute to the pH, while a large amount of H$^+$ counterions are closely associated with the hybrids. (If protons are free in solution, the molar ratio should be 0.5). When dilute NaOH solution is slowly titrated into the solution of POM hybrid, a gradual decrease of the excimer peak along with a continuous increase in the pyrene monomer peaks occurs, indicating that the distance between pyrene excimers increases (larger than 0.5 nm). Because Na$^+$ has a weaker affinity for the hybrid macroanions in solution than H$^+$ does,[58] which leads to less screening of the POM cluster from neighboring groups, the drop of proton concentration in solution will increase the repulsion between adjacent POM groups in the vesicles. When the solution pH approaches 7, the decrease in the ratio of

Scheme 2. Illustration of Possible Vesicular Structures Formed by Hybrid Clusters, 2, in Polar Solvents, and How the TBA Counterions May Be Arranged in the Packing of Individual Clusters[a]
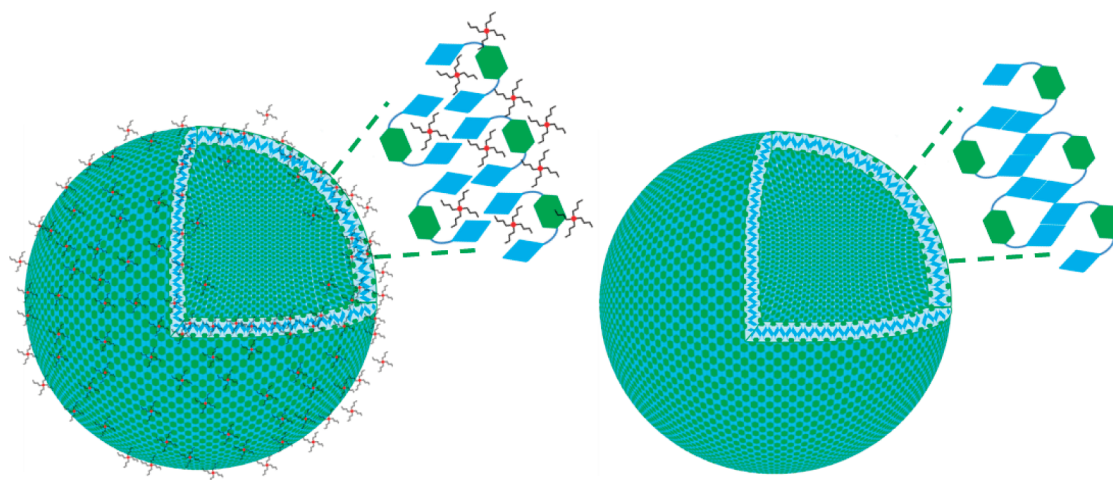
[a] The hexagons, parallelograms, and four-legged stars represent the POM, pyrene, and TBA cations, respectively.
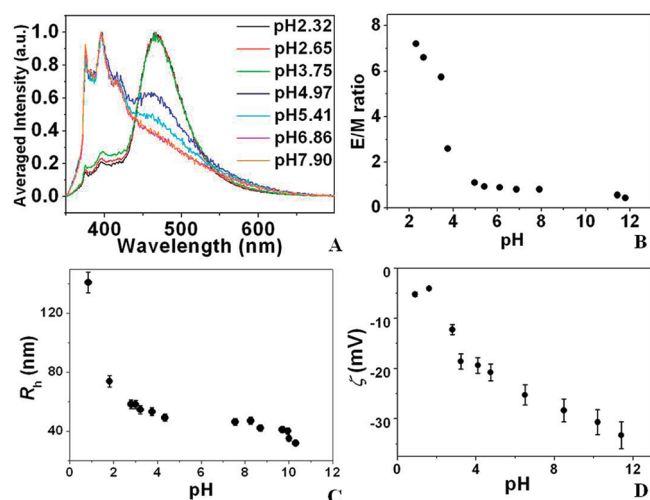

Figure 4. (A) Fluorescence spectra of hybrid clusters $(H^+)_2\mathbf{2}$ in water at different pH values (the fluorescence intensity has been normalized). (B) Plot of pyrene excimer/monomer intensity ratio versus solution pH for hybrid clusters $(H^+)_2\mathbf{2}$. (C) Change in the vesicular structure size with solution pH for $(H^+)_2\mathbf{2}$. (D) Zeta potential of the vesicular structure with solution pH for $(H^+)_2\mathbf{2}$. The sample concentration of ~0.4 mg/mL was determined by UV absorption.

[excimer]/[monomer] peak areas becomes much slower, indicating that the distance between hybrid clusters becomes less sensitive to pH due to the limited amount of available protons. More interestingly, in the pH range of 1–7, the whole process is reversible. In other words, the average pyrene-to-pyrene distance between adjacent clusters is reversibly tunable by changing pH.

The average vesicle size recorded by DLS at 90° scattering angle also shows pH dependence: the R_h of vesicles decreases with increasing pH. Stronger electrostatic repulsion between hybrid clusters will result in a high curvature, that is, a smaller vesicle, for the assemblies; this trend shows how counterions affect the close packing of hybrid clusters. Meanwhile, the zeta potential of the vesicular structures becomes more negative with increasing pH and becomes nearly neutral at a low pH,

indicating that the net charge on the vesicles increases with increasing pH.

■ CONCLUSIONS

In summary, two novel POM-based hybrid clusters were synthesized by connecting one or two organic pyrene tails with a Lindqvist type polyoxovanadate head cluster through triester capping groups. These two hybrid clusters demonstrate noteworthy amphiphilic properties by forming spherical vesicular structures in polar solvents. Four different counterions (TBA, TEA, TMA, and H^+) have been used to study the counterion effect on the vesicular structures and their consequent role in the fluorescent properties of the pyrene groups on vesicle surface. TBA counterions not only interact with POM polar head groups but also move into the hydrophobic regions and interrupt the close packing of pyrene groups. More importantly, when TBA counterions are replaced by protons, a dramatic change of the pyrene fluorescence pattern occurs, and the vesicle size, the fluorescence pattern, and the effective charge on the vesicles change correspondingly and reversibly with solution pH. The construction of pH sensitive vesicular structures could well have application to artificial cell studies, nanoreactors, as well as drug and gene delivery systems.

■ ASSOCIATED CONTENT

ⓢ **Supporting Information.** Crystallographic data for TBA, $(TBA^+)_2\mathbf{1}$, and $(TBA^+)_2\mathbf{2}$. Details of the synthesis and characterization of $(TBA^+)_2\mathbf{1}$ and $(TBA^+)_2\mathbf{2}$, vesicle characterization, counterion exchange, and pH effects. This information is available free of charge via the Internet at http://pubs.acs.org/.

■ AUTHOR INFORMATION

Corresponding Author
liu@lehigh.edu; chill@emory.edu

Author Contributions
[§]These two authors contributed equally to this paper.

14015

dx.doi.org/10.1021/ja204034g |*J. Am. Chem. Soc.* 2011, 133, 14010–14016

■ REFERENCES

(1) Lee, E.; Kim, J.-K.; Lee, M. *Macromol. Rapid Commun.* **2010**, *31*, 975.

(2) Li, M.-H.; Keller, P. *Soft Matter* **2009**, *5*, 927.

(3) Zhang, X.; Rehm, S.; Safont-Sempere, M. M.; Würthner, F. *Nat. Chem.* **2009**, *1*, 623.

(4) Roberts, M. C.; Hanson, M. C.; Massey, A. P.; Karren, E. A.; Kiser, P. F. *Adv. Mater.* **2007**, *19*, 2503.

(5) Wang, M.-S.; Xu, G.; Zhang, Z.-J.; Guo, G.-C. *Chem. Commun.* **2010**, *46*, 361.

(6) Bardelang, D.; Zaman, M. B.; Moudrakovski, I. L.; Pawsey, S.; Margeson, J. C.; Wang, D.; Wu, X.; Ripmeester, J. A.; Ratcliffe, C. I.; Yu, K. *Adv. Mater.* **2008**, *20*, 4517.

(7) Katagiri, K.; Nakamura, M.; Koumoto, K. *ACS Appl. Mater.* **2010**, *2*, 768.

(8) Hu, J.; Liu, S. *Macromolecules* **2010**, *43*, 8315.

(9) Haag, R. *Angew. Chem., Int. Ed.* **2004**, *43*, 278.

(10) Griset, A. P.; Walpole, J.; Liu, R.; Gaffey, A.; Colson, Y. L.; Grinstaff, M. W. *J. Am. Chem. Soc.* **2009**, *131*, 2469.

(11) Aryal, S.; Hu, C.-M. J.; Zhang, L. *ACS Nano* **2009**, *4*, 251.

(12) Shi, N. E.; Dong, H.; Yin, G.; Xu, Z.; Li, S. H. *Adv. Funct. Mater.* **2007**, *17*, 1837.

(13) Ali, M.; Yameen, B.; Cervera, J.; Ramírez, P.; Neumann, R.; Ensinger, W.; Knoll, W.; Azzaroni, O. *J. Am. Chem. Soc.* **2010**, *132*, 8338.

(14) Wang, R.; Jiang, X.; Di, C.; Yin, J. *Macromolecules* **2010**, *43*, 10628.

(15) Müller, A.; Peters, F. *Chem. Rev.* **1998**, *98*, 239.

(16) Long, D. L.; Burkholder, E.; Cronin, L. *Chem. Soc. Rev.* **2007**, *36*, 105.

(17) Rhule, J. T.; Hill, C. L.; Judd, D. A.; Schinazi, R. F. *Chem. Rev.* **1998**, *98*, 327.

(18) Yin, P.; Wu, P.; Xiao, Z.; Li, D.; Bitterlich, E.; Zhang, J.; Cheng, P.; Vezenov, D. V.; Liu, T.; Wei, Y. *Angew. Chem., Int. Ed.* **2011**, *50*, 2521.

(19) Dolbecq, A.; Dumas, E.; Mayer, C. d. R.; Mialane, P. *Chem. Rev.* **2010**, *110*, 6009.

(20) Xu, L.; Lu, M.; Xu, B.; Wei, Y.; Peng, Z.; Powell, D. R. *Angew. Chem., Int. Ed.* **2002**, *41*, 4129.

(21) Mayer, C. R.; Cabuil, V.; Lalot, T.; Thouvenot, R. *Angew. Chem., Int. Ed.* **1999**, *38*, 3672.

(22) Song, Y.-F.; McMillan, N.; Long, D.-L.; Kane, S.; Malm, J.; Riehle, M. O.; Pradeep, C. P.; Gadegaard, N.; Cronin, L. *J. Am. Chem. Soc.* **2009**, *131*, 1340.

(23) Khan, M. I.; Chen, Q.; Goshorn, D. P.; Hope, H.; Parkin, S.; Zubieta, J. *J. Am. Chem. Soc.* **1992**, *114*, 3341.

(24) Chen, Q.; Goshorn, D. P.; Scholes, C. P.; Tan, X. L.; Zubieta, J. *J. Am. Chem. Soc.* **1992**, *114*, 4667.

(25) Gouzerh, P.; Proust, A. *Chem. Rev.* **1998**, *98*, 77.

(26) Proust, A.; Thouvenot, R.; Gouzerh, P. *Chem. Commun.* **2008**, 1837.

(27) Joo, N.; Renaudineau, S.; Delapierre, G.; Bidan, G.; Chamoreau, L.-M.; Thouvenot, R.; Gouzerh, P.; Proust, A. *Chem.—Eur. J.* **2010**, *16*, 5043.

(28) Bar-Nahum, I.; Cohen, H.; Neumann, R. *Inorg. Chem.* **2003**, *42*, 3677.

(29) Hou, Y.; Hill, C. L. *J. Am. Chem. Soc.* **1993**, *115*, 11823.

(30) Zeng, H.; Newkome, G. R.; Hill, C. L. *Angew. Chem., Int. Ed.* **2000**, *39*, 1771.

(31) Bar-Nahum, I.; Khenkin, A. M.; Neumann, R. *J. Am. Chem. Soc.* **2004**, *126*, 10236.

(32) Weiner, H.; Hayashi, Y.; Finke, R. G. *Inorg. Chem.* **1999**, *38*, 2579.

(33) Yan, Y.; Wang, H.; Li, B.; Hou, G.; Yin, Z.; Wu, L.; Yam, V. W. W. *Angew. Chem., Int. Ed.* **2010**, *49*, 9233.

(34) Carlisle, R. C.; Osburn Atkinson, E. J.; McAdams, D.; Hayden, E. J.; Ankeny Brown, D. J. *Chem. Commun.* **2003**, 2456.

(35) Landsmann, S.; Lizandara-Pueyo, C.; Polarz, S. *J. Am. Chem. Soc.* **2010**, *132*, 5315.

(36) Rosnes, M. H.; Musumeci, C.; Pradeep, C. P.; Mathieson, J. S.; Long, D.-L.; Song, Y.-F.; Pignataro, B.; Cogdell, R.; Cronin, L. *J. Am. Chem. Soc.* **2010**, *132*, 15490.

(37) Zhang, J.; Liu, T.; Mal, S. S.; Kortz, U. *Eur. J. Inorg. Chem.* **2010**, *2010*, 3195.

(38) Zhang, J.; Song, Y.-F.; Cronin, L.; Liu, T. *Chem.—Eur. J.* **2010**, *16*, 11320.

(39) Pradeep, C. P.; Misdrahi, M. F.; Li, F.-Y.; Zhang, J.; Xu, L.; Long, D.-L.; Liu, T.; Cronin, L. *Angew. Chem., Int. Ed.* **2009**, *48*, 8309.

(40) Winnik, F. M. *Chem. Rev.* **1993**, *93*, 587.

(41) Kalyanasundaram, K.; Thomas, J. K. *J. Am. Chem. Soc.* **1977**, *99*, 2039.

(42) Glushko, V.; Thaler, M. S. R.; Karp, C. D. *Arch. Biochem. Biophys.* **1981**, *210*, 33.

(43) Bruker AXS, I., 5.628 ed.; Analytical X-ray Systems: Madison, WI, 2003.

(44) Bruker AXS, I., 6.45 ed.; Analytical X-ray Systems: Madison, WI, 2003.

(45) Hiemenz, P. C.; Rajagopalan, R. *Principles of Colloid and Surface Chemistry*, 3rd ed.; CRC Press: New York, 1997.

(46) Liu, T.; Diemann, E.; Li, H.; Dress, A. W. M.; Müller, A. *Nature* **2003**, *426*, 59.

(47) Discher, D. E.; Eisenberg, A. *Science* **2002**, *297*, 967.

(48) Mecke, A.; Dittrich, C.; Meier, W. *Soft Matter* **2006**, *2*, 751.

(49) Nandi, N.; Vollhardt, D. *Acc. Chem. Res.* **2007**, *40*, 351.

(50) Song, J.; Luo, Z.; Zhu, H.; Huang, Z.; Lian, T.; Kaledin, A. L.; Musaev, D. G.; Lense, S.; Hardcastle, K. I.; Hill, C. L. *Inorg. Chim. Acta* **2010**, *363*, 4381.

(51) Beck, P.; Liebi, M.; Kohlbrecher, J.; Ishikawa, T.; Rüegger, H.; Zepik, H.; Fischer, P.; Walde, P.; Windhab, E. *J. Phys. Chem. B* **2009**, *114*, 174.

(52) Zhang, J.; Song, Y.-F.; Cronin, L.; Liu, T. *J. Am. Chem. Soc.* **2008**, *130*, 14408.

(53) Ernst, R. R.; Bodenhausen, G.; Wokaun, A. *Principles of Nuclear Magnetic Resonance in One and Two Dimensions*; Oxford University Press: Oxford, U.K., 1992.

(54) Hassinen, A.; Moreels, I.; de Mello Donegá, C.; Martins, J. C.; Hens, Z. *J. Phys. Chem. Lett.* **2010**, *1*, 2577.

(55) Denkova, P. S.; Van Lokeren, L.; Willem, R. *J. Phys. Chem. B* **2009**, *113*, 6703.

(56) Yuan, H.-Z.; Cheng, G.-Z.; Zhao, S.; Miao, X.-J.; Yu, J.-Y.; Shen, L.-F.; Du, Y.-R. *Langmuir* **2000**, *16*, 3030.

(57) Cros-Gagneux, A.; Delpech, F.; Nayral, C. l.; Cornejo, A.; Coppel, Y.; Chaudret, B. *J. Am. Chem. Soc.* **2010**, *132*, 18147.

(58) Pigga, J. M.; Teprovich, J. A.; Flowers, R. A.; Antonio, M. R.; Liu, T. *Langmuir* **2010**, *26*, 9449.